

Self-Sustained Spin-Polarized Current Oscillations in Diluted Magnetic Semiconductor Superlattices

Manuel Carretero^{1,2}, Ramón Escobedo³, Luis L. Bonilla^{1,2}, and Gloria Platero⁴

¹G. Millán Institute, Fluid Dynamics, Nanoscience & Industrial Mathematics, Universidad Carlos III, 28911 Leganés, Spain

²Unidad Asociada al Instituto de Ciencia de Materiales de Madrid, CSIC, 28911 Madrid, Spain

³Departamento de Matemática Aplicada y Ciencias de la Computación, Universidad de Cantabria, 39005 Santander, Spain

⁴Instituto de Ciencia de Materiales, CSIC, 28049 Cantoblanco, Spain

A direct current (dc) voltage biased II-VI semiconductor multi-quantum well structure attached to normal contacts exhibits self-sustained spin-polarized current oscillations if one or more of its wells are doped with Mn. Self-sustained current oscillations are due to repeated triggering of charge dipole domains at the magnetic wells and motion towards the collector. Without magnetic impurities, the only configurations appearing in these structures are stationary. Analysis and numerical solution of a nonlinear spin transport model yield the minimal number of wells and the range of doping density needed to find oscillations, the current-voltage characteristic curve and the main features of stable stationary and time-periodic states. Our study could allow designing the oscillatory spin-polarized current injectors.

Index Terms—Diluted magnetic semiconductor superlattices, self-sustained current oscillations, spintronics.

I. INTRODUCTION

SEMICONDUCTORS with nonlinear current-voltage characteristics are promising materials for spintronics applications [1]. Diluted magnetic semiconductors (DMSs) are efficient spin injectors as it has been shown by using contacts based in Mn [2], [3]. Electrical injection of spin-polarized current makes DMS nanostructures interesting potential spintronic devices [2], [4]. Carrier-ion exchange spin effects dominate the magnetotransport in II-VI-based semiconductor multi-quantum-well structures (MQWS) doped with Mn⁺⁺ ions, producing spin-polarized transport and large magnetoresistance [5]. Exchange interaction between the spin carrier and Mn ions results in large spin splittings. In fact, full spin polarization has been achieved at magnetic fields of 1 T. Recently [6]–[8], nonlinear transport through DMS superlattices (SL) has been investigated. The interplay between the nonlinearity of the current-voltage characteristics and the exchange interaction produces interesting spin-dependent features: multistability of steady states with different polarization in the magnetic wells [6], time-periodic oscillations of the spin-polarized current, and induced spin polarization in nonmagnetic wells by their magnetic neighbors [8], among others. The high sensitivity of these systems to external fields points out to their potential application as magnetic sensors [6] whereas four-period devices may inject spin-polarized electrons and current and act as spin oscillators [8].

In this paper, we describe the current-voltage (I-V) characteristic curve of an *n*-doped ZnSe/(Zn,Cd,Mn)Se weakly coupled SL whose first quantum well (QW) is doped with Mn. Besides regions where a direct current (dc) voltage bias yields a dc current as response, there are voltage intervals where a stable time-periodic oscillation of the current is the response to a dc bias. These so-called self-sustained current oscillations (SSCOs) are due to the periodic generation and motion of high

electric field domains at the QWs containing magnetic impurities. The electrostatic nature of these electric field domains make them quite different from the magnetic domains usually found in ferromagnetic materials. The rich nonlinear dynamics of electric field domains is reminiscent of that found in conventional weakly coupled semiconductor SL [9]–[11]. We also describe the field, polarization, current, and electron densities in the different regions of the I-V curve.

II. MODEL

The spin for the magnetic ion Mn⁺⁺ is $S = 5/2$ and the exchange interaction between the Mn local moments and the conduction band electrons is ferromagnetic in II-VI QWs. Using the virtual crystal and mean field approximations, the effect of the exchange interaction is to make the subband energies spin dependent in those QWs that contain Mn ions: $E_j^\pm = E_j \mp \Delta/2$ where $\Delta = 2J_{sd}N_{Mn}SB_S(g\mu_B B_S/(k_B T_{eff}))$ for spin $s = \pm 1/2$, and B , J_{sd} , N_{Mn} , k_B , and T_{eff} are the external magnetic field, the exchange integral, the density of magnetic impurities, the Boltzmann constant, and an effective temperature, which accounts for Mn interactions, respectively [6]. We model spin-flip scattering coming from spin-orbit or hyperfine interaction through a phenomenological scattering time τ_{sf} , which is larger than impurity and phonon scattering times: $\tau_{scat} = \hbar/\gamma < \tau_{sf}$. Vertical transport in the nanostructure is spin-independent sequential tunneling between adjacent QWs, so when electrons tunnel to an excited state they instantaneously relax by phonon scattering to the ground state with the same spin polarization. Last, electron-electron interaction is considered within the Hartree mean field approximation. The equations describing our model are [8]

$$F_i - F_{i-1} = \frac{e}{\epsilon} (n_i^+ + n_i^- - N_D) \quad (1)$$

$$e \frac{dn_i^\pm}{dt} = J_{i-1 \rightarrow i}^\pm - J_{i \rightarrow i+1}^\pm \pm \frac{n_i^- - n_i^+}{\tau_{sf}} \Theta_i \quad (2)$$

$$\Theta_i = 1 + e^{\frac{E_{1,i}^- - \mu_i^+}{\gamma\mu}} \quad (3)$$

where $i = 1, \dots, N$, n_i^+ , n_i^- , and $-F_i$ are the 2-D spin-up and spin-down electron densities, and the average electric field at

Digital Object Identifier 10.1109/TMAG.2008.2002371

Color versions of one or more of the figures in this paper are available online at <http://ieeexplore.ieee.org>.

the i th SL period (which starts at the right end of the $(i - 1)$ th barrier and finishes at the right end of the i th barrier), respectively. The voltage bias condition is $\sum_{i=0}^N F_i l = V$ for the applied voltage V . We have denoted the spin-dependent subband energies (E) (measured from the bottom of the i th well) by $E_{j,i}^{\pm} = E_j \mp \Delta_i/2$, with $\Delta_i = \Delta$ or 0 , depending on whether the i th well contains magnetic impurities. N_D , ε , $-e$, $l = d + w$, and $-J_{i \rightarrow i+1}^{\pm}$ are the 2-D doping density at the QWs, the average permittivity, the electron charge, the width of an SL period (d and w are barrier and well widths), and the tunneling current density across the i th barrier, respectively. For electrons with spin $\pm 1/2$, the chemical potentials at the i th SL period, μ_i^{\pm} , are related to the electron densities by

$$n_i^{\pm} = \frac{m^* k_B T}{2\pi \hbar^2} \ln \left[1 + \exp \left(\frac{\mu_i^{\pm} - E_{1,i}^{\pm}}{k_B T} \right) \right]. \quad (4)$$

Here, m^* is the effective electron mass. For numerical convenience, the right-hand side of (2) contains a smoothed form of the scattering term used in [6]. As $\gamma_{\mu} \rightarrow 0$, our scattering term becomes $\pm(n_i^- - n_i^+)/\tau_{sf}$ for $\mu_i^+ > E_{1,i}^-$ (equivalently, $\mu_i^+ - E_{1,i}^+ > \Delta$), and $\pm n_i^-/\tau_{sf}$, otherwise [6]. Time-differencing (1) and inserting (2) in the result, we obtain the following form of Ampère's law:

$$\varepsilon \frac{dF_i}{dt} + J_{i \rightarrow i+1} = J(t) = \frac{1}{N+1} \sum_{i=0}^N J_{i \rightarrow i+1} \quad (5)$$

where $J_{i \rightarrow i+1} = J_{i \rightarrow i+1}^+ + J_{i \rightarrow i+1}^-$. In (5), $J(t)$ (independent of i) is the total current density. The formula $J(t) = \sum_{i=0}^N J_{i \rightarrow i+1}/(N+1)$ is found by adding (5) for all i and using $dV/dt = l \sum_{i=0}^N dF_i/dt = 0$. Tunneling currents are calculated by the transfer Hamiltonian method taking into account that spin-up and spin-down electrons have different energies

$$J_{i \rightarrow i+1}^{\pm} = \frac{ev^{(f)\pm}(F_i)}{l} \left\{ n_i^{\pm} - \frac{m^* k_B T}{2\pi \hbar^2} \ln \left[1 + e^{-\frac{eF_i l}{k_B T}} \left(\exp \left(\frac{2\pi \hbar^2 n_{i+1}^{\pm}}{m^* k_B T} \right) - 1 \right) \right] \right\} \quad (6)$$

for $i = 1, \dots, N - 1$, provided that scattering-induced broadening of energy levels is much smaller than subband energies and chemical potentials [11]. As boundary tunnelling currents for $i = 0$ and N , we use (6) with $n_0^{\pm} = n_{N+1}^{\pm} = \kappa N_D/2$ (identical normal contacts with $\kappa \geq 1$) [6]. Initially, we set $F_i = V/[l(N+1)]$, $n_i^{\pm} = N_D/2$ (normal QWs). The spin-dependent "forward tunneling velocity" $v^{(f)\pm}$ is a sum of Lorentzians of width 2γ (the same value for all subbands, for simplicity) centered at the resonant field values $F_{j,i}^{\pm} = (E_{j,i}^{\pm} - E_{1,i}^{\pm})/(el)$ [11]

$$v^{(f)\pm}(F_i) = \sum_{j=1}^2 \frac{\hbar^3 l \gamma}{2\pi^2 m^{*2}} \mathcal{T}_i(E_{1,i}^{\pm})}{(E_{1,i}^{\pm} - E_{j,i+1}^{\pm} + eF_i l)^2 + (2\gamma)^2}. \quad (7)$$

Here, \mathcal{T}_i is proportional to the dimensionless transmission probability across the i th barrier [11]. Equations (6) and (7) are the same as in [11, App. A] except for factors of 2 due to

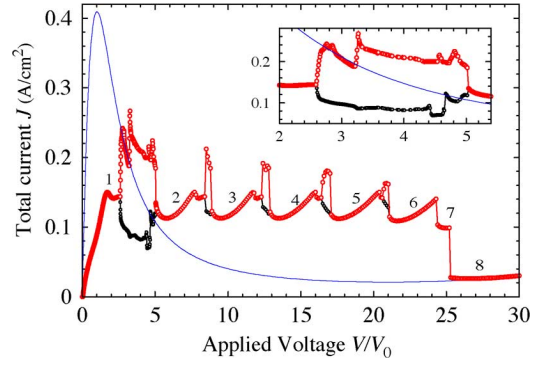


Fig. 1. Current-voltage characteristics for an 8-period SL with $\Delta = 12$ meV. The maximum and minimum of the SSCOs has been represented in each voltage interval where they exist. The superimposed thin solid line represents the current (6) for $n_i^{\pm} = N_D/2$, $F_i = F$. The first interval of current oscillations is shown in the inset. Here $V_0 = (N + 1)F_M l = 8.64$ mV.

spin polarization. A factor $1/(2\pi^2)$ has been included in (7) to recover in the zero temperature limit the same values as in [6]. The tunneling current densities $J_{i \rightarrow i+1}^{\pm}$ are functions $J_{i \rightarrow i+1}^{\pm}(F_i, n_i^{\pm}, n_{i+1}^{\pm})$ of F_i , n_i^{\pm} , and n_{i+1}^{\pm} . For constant values $n_i^{\pm} = N_D/2$ and $F_i = F$, the tunneling current density at a nonmagnetic QW has a maximum J_M at a value F_M of the field. In terms of F_M , the voltage bias condition can be written as a condition for the average field ϕ

$$\frac{1}{(N+1)F_M} \sum_{i=0}^N F_i = \phi \equiv \frac{V}{(N+1)F_M l}. \quad (8)$$

To recover voltage from the dimensionless bias, we have to multiply ϕ by $V_0 = (N+1)F_M l$.

III. STATIONARY STATES AND SELF-SUSTAINED OSCILLATIONS

For typical values of the parameters, the model governed by (1)–(8) exhibits a variety of stationary states with electric field domains [6] and SSCOs [8]. We have considered a sample with $N = 8$ QW, $l = 15$ nm (corresponding to barrier and well widths of 10 and 5 nm, respectively), $N_D = 10^{10}$ cm $^{-2}$, $\tau_{sf} = 10^{-9}$ s (normal QW) [12] and 10^{-11} s (magnetic QW) [13], $m^* = 0.16m_0$, $\varepsilon = 7.1\varepsilon_0$, $T = 5$ K, $E_1 = 15.76$ meV, $E_2 = 61.99$ meV, $\gamma = 1$ meV, $\gamma_{\mu} = 0.1$ meV, and $\kappa = 1$. For these values, $J_M = 0.409$ A/cm 2 , $F_M = 0.64$ kV/cm, and $V_0 = 9F_M l = 8.64$ mV. Only the first QW contains magnetic impurities yielding a spin splitting $\Delta = 12$ meV.

A. Current-Voltage Characteristics

As explained in [8], SSCOs appear when the SL has at least four QWs and the doping density in them surpasses a first critical value that depends on the number of wells N as $N_{D,1} = 2/(N-2) \times 10^{10}$ cm $^{-2}$. For $N_D = 10^{10}$ cm $^{-2}$, there are SSCOs for values of the dimensionless average field (8) in several intervals, which we denote by $\phi_{\alpha,k}^N < \phi < \phi_{\omega,k}^N$, $k = 1, 2, \dots$, and whose number and width depend on N . The first bias interval for which there are SSCOs is the widest. For $N = 8$, this interval is $2.59 < \phi < 5.04$. The current-voltage characteristics for an 8-period SL is depicted in Fig. 1, in which we show the maximum and minimum values of the current during SSCOs for biases in the voltage intervals $(\phi_{\alpha,k}, \phi_{\omega,k})$, $k = 1, \dots, 5$.

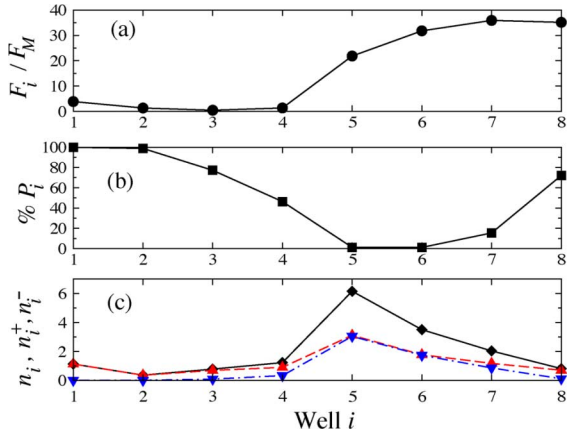


Fig. 2. Stationary profiles of the electric field, polarization, and electron densities $n_i = n_i^+ + n_i^-$ (solid line), n_i^+ (dashed line, triangles), and n_i^- (dotted-dashed line, inverted triangles) for a bias $\phi = 15$.

B. Stationary States

The stationary states for $\phi < \phi_{\alpha,1}$ and for $\phi > \phi_{\omega,5}$ (the last oscillation interval) are spatially almost uniform

$$\frac{F_i}{F_M} = \phi$$

$$J = J_{i \rightarrow i+1}^+ \left(F_M \phi, \frac{1+P}{2} N_D, \frac{1+P}{2} N_D \right) + J_{i \rightarrow i+1}^- \left(F_M \phi, \frac{1-P}{2} N_D, \frac{1-P}{2} N_D \right) \quad (9)$$

where P is the uniform value of the polarization

$$P_i = \frac{n_i^+ - n_i^-}{n_i^+ + n_i^-}. \quad (10)$$

Note that the tunneling currents from the first to the second QW are different from all others because only the first QW contains magnetic impurities. It turns out that $P \approx 0.6$, so that the QW polarization at the almost uniform state is 60% and the lower energy state is more populated, with $n^+ = 0.8N_D$, than the higher energy state, with $n^- = 0.2N_D$.

In the other stationary intervals of the I-V diagram, the profiles of F_i , P_i , and n_i^\pm are not uniform as shown in Fig. 2. There are two electric field domains, a low field domain adjacent to the cathode and a high field domain that extends to the anode, separated by a domain wall in which the field increases. For larger bias, the domain wall moves closer to the injecting contact but domain walls cannot start at the QW $i = 2$ adjacent to the magnetic QW $i = 1$, and at $i = N - 1$ due to the boundary condition at $i = N$. There are N voltage intervals of stationary solution branches in Fig. 1, including the almost uniform branches before the first and after the last interval of SSCO. The polarization drops to zero in the QW located after the domain wall and then it increases in the high field domain. A comparison of the electric field profile containing two domains and the almost uniform field profiles before the first and after the last oscillation intervals is shown in Fig. 3.

C. Self-Sustained Oscillations

The first voltage interval of SSCOs in Fig. 1 is the widest. Within this interval, the function $J(t)$ adopts different shapes as ϕ increases, as depicted in Fig. 4.

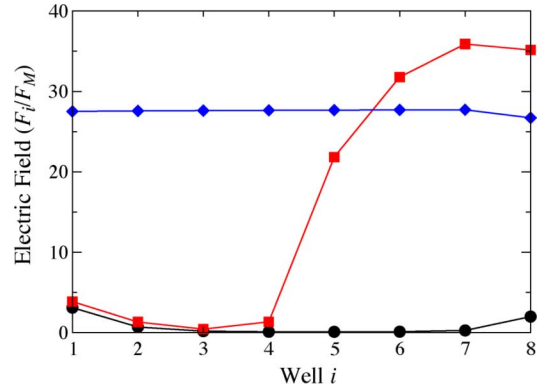


Fig. 3. Field profile of the stable stationary state for $\phi = 1$ (circles), 15 (squares), and 27 (diamonds).

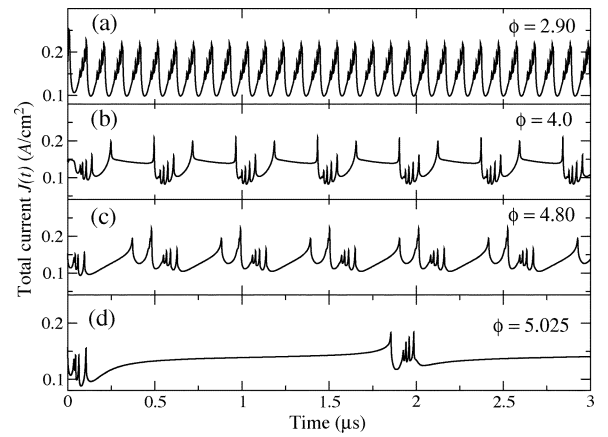


Fig. 4. Total current density versus time for different biases in the first voltage interval of SSCOs in Fig. 1.

- For $\phi \in (2.59, 3.2)$, the field profiles corresponding to Fig. 4(a) consist of the repeated nucleation of a charge dipole wave at the magnetic QW, its motion towards the anode, its arrival and growth there, and the appearance of a new wave when the current reaches a critical value. This is similar to the Gunn effect in bulk semiconductors [14]. For ϕ slightly larger than 2.59, the dipole waves periodically nucleated at the magnetic QW are attenuated and disappear inside the SL, which provides an almost sinusoidal current oscillation. This scenario is similar to a Gunn effect confined to part of the structure [15].
- At $\phi = 3.2$, the maximum value of the current increases abruptly; see the inset of Fig. 1. The field at the end of the SL becomes larger than the maximum value of the field at the moving dipole wave. This occurs for $\phi \in (3.2, 5.0)$, a voltage interval in which the travel time of the dipole wave remains about the same while the time to nucleate a new wave increases with ϕ . See Fig. 4(b) and (c).
- For $\phi \in (5.0, 5.04)$, the nucleation time for new dipole waves is very long and it increases with ϕ . During this time, the field profile resembles very much the profile of the nonuniform stationary state at the branch marked 2 in Fig. 1 (similar to that marked with squares in Fig. 3 but the domain wall starts at $i = 6$ instead of $i = 4$). The wave nucleation time increases until it becomes infinite at $\phi_{\omega,1}^N = 5.04$ and then the stationary state corresponding to branch 2 in Fig. 1 is reached; see Fig. 4(d) and compare it

to Fig. 4(c). This scenario corresponds to a collision of the branch of SSCO with a homoclinic orbit of the stationary state.

The mechanism of wave triggering at the magnetic QW is described in [8]. At the magnetic QW, the total tunneling current density has a first maximum for positive values of the field, which is displaced to larger field values with respect to the maximum tunneling current density for nonmagnetic QWs provided the electron densities are kept constant at zero polarization. In fact, the corresponding current-field curves intersect at the decreasing part of the tunneling current for nonmagnetic field, after its maximum value. This intersection point defines critical values of the current density and of the field. Then, the field at the magnetic QW is larger than the field at the successive QWs provided the total current density is lower than the critical current. Whenever the total current density surpasses the critical current density, a charge dipole wave (high electric field domain) is nucleated at the magnetic QW. As in the case of the Gunn effect in bulk semiconductors [14], a single dipole wave far from the magnetic QW moves towards the anode and the total current density is smaller than the critical current density. As the dipole reaches the anode and starts disappearing, $J(t)$ increases so as to keep the voltage constraint (8). As $J(t)$ surpasses the critical value, a new dipole wave is nucleated at the magnetic QW and the total current density drops again below its critical value. The area lost by the dipole wave disappearing at the anode is gained by the newly nucleated one and the cycle repeats itself.

IV. CONCLUSION

We have studied the phase diagram, current-voltage characteristics, and SSCOs for an SL whose first QW is doped with magnetic impurities. For appropriate values of the doping density, several voltage intervals for which there are stable SSCOs are separated by intervals of stable stationary states. The first voltage interval of SSCOs is the widest and SSCOs are due to periodic triggering of dipole waves at the magnetized QW. In this interval, the motion of dipoles is confined to part of the structure for lower voltages and it arrives at the structure end for intermediate voltages. For larger voltages, there is a charge accumulation at the end of the SL and motion of dipoles is confined between the magnetized well and the charge accumulation layer. The branch of SSCOs ends by its collision with a homoclinic orbit of the stationary state. To understand the SSCOs, we have to realize that the magnetized well acts as a boundary condition creating a charge depletion layer in its neighborhood. When the tunneling current density from this well reaches the same value as the total current density, a dipole wave is nucleated there and released afterwards when these two currents again coincide.

During SSCOs, QWs are fully polarized when the dipole wave is traversing them. Therefore, a short device would periodically inject pulses of polarized current to the collector. It is important that normal contacts can be used to build the oscillator, because the crucial requirement is to dope the first QW with Mn. We have also indicated the range of doping

density needed to achieve spin-polarized SSCOs. For self-oscillations to occur, appropriate ranges of spin splitting should be induced by tailoring the magnetic impurity density and external magnetic fields. Our results could be used to construct an oscillatory spin-polarized current injector.

ACKNOWLEDGMENT

This work was supported by the MECD grants MAT2005-05730-C02-01 and MAT2005-06444. R. Escobedo would like to thank the Ramón y Cajal Program of the Spanish Ministry of Education and Science.

REFERENCES

- [1] I. Zutic, J. Fabian, and S. Das Sarma, "Spintronics: Fundamentals and applications," *Rev. Mod. Phys.*, vol. 76, pp. 323–410, 2004.
- [2] A. Khaetskii, J. C. Egues, D. Loss, C. Gould, G. Schmidt, and L. W. Molenkamp, "Spin injection across magnetic/nonmagnetic interfaces with finite magnetic layers," *Phys. Rev. B, Condens. Matter*, vol. 71, pp. 235327-1–235327-6, 2005.
- [3] A. Slobodskyy, C. Gould, T. Slobodskyy, G. Schmidt, L. W. Molenkamp, and D. Sánchez, "Resonant tunneling diode with spin polarized injector," *Appl. Phys. Lett.*, vol. 90, pp. 122109-1–122109-3, 2007.
- [4] F. Mireles and G. Kirzenow, "Coherent spin-valve phenomena and electrical spin injection in ferromagnetic/semiconductor/ferromagnetic junctions," *Phys. Rev. B, Condens. Matter*, vol. 66, pp. 214415-1–214415-13, 2002.
- [5] S. A. Crooker, D. A. Tulchinsky, J. Levy, D. D. Awschalom, R. Garcia, and N. Samarth, "Enhanced spin interactions in digital magnetic heterostructures," *Phys. Rev. Lett.*, vol. 75, pp. 505–508, 1995.
- [6] D. Sánchez, A. H. MacDonald, and G. Platero, "Field-domain spintronics in magnetic semiconductor multiple quantum wells," *Phys. Rev. B, Condens. Matter*, vol. 65, p. 035301, 2002.
- [7] M. Béjar, D. Sánchez, G. Platero, and A. H. MacDonald, "Spin-polarized current oscillations in diluted magnetic semiconductor multiple quantum wells," *Phys. Rev. B, Condens. Matter*, vol. 67, pp. 045324-1–045324-5, 2003.
- [8] L. L. Bonilla, R. Escobedo, M. Carretero, and G. Platero, "Multiquantum well spin oscillator," *Appl. Phys. Lett.*, vol. 91, pp. 092102-1–092102-3, 2007.
- [9] L. L. Bonilla and H. T. Grahn, "Nonlinear dynamics of semiconductor superlattices," *Rep. Prog. Phys.*, vol. 68, pp. 577–683, 2005.
- [10] G. Platero and R. Aguado, "Photon-assisted transport in semiconductor nanostructures," *Phys. Rep.*, vol. 395, pp. 1–157, 2004.
- [11] L. L. Bonilla, "Theory of nonlinear charge transport, wave propagation and self-oscillations in semiconductor superlattices," *J. Phys. Cond. Matter*, vol. 14, pp. R341–R381, 2002.
- [12] J. M. Kikkawa, I. P. Smorchkova, N. Samarth, and D. D. Awschalom, "Room-temperature spin memory in two-dimensional electron gases," *Science*, vol. 277, pp. 1284–1287, Aug. 29, 1997.
- [13] D. D. Awschalom and N. Samarth, "Spin dynamics and quantum transport in magnetic semiconductor quantum structures," *J. Magn. Mater.*, vol. 200, pp. 130–147, October 1999.
- [14] H. Kroemer, "Gunn effect—Bulk instabilities," in *Topics in Solid State and Quantum Electronics*, W. D. Hershberger, Ed. New York: Wiley, 1972, pp. 20–98.
- [15] L. L. Bonilla, R. Escobedo, and F. J. Higuera, "Axisymmetric pulse recycling and motion in bulk semiconductors," *Phys. Rev. E, Stat. Phys. Plasmas Fluids Relat. Interdiscip. Top.*, vol. 65, pp. 016607-1–016607-8, 2001.

Manuscript received February 28, 2008. Current version published December 17, 2008. Corresponding author: M. Carretero (e-mail: manuel.carretero@uc3m.es).